Highly Robust Indium-Free Transparent Conductive Electrodes Based on Composites of Silver Nanowires and Conductive Metal Oxides

*Kirill Zilberberg, Felix Gasse, Richie Pagui, Andreas Polywka, Andreas Behrendt, Sara Trost, Ralf Heiderhoff, Patrick Görrn, and Thomas Riedl**

A hybrid approach for the realization of In-free transparent conductive layers based on a composite of a mesh of silver nanowires (NWs) and a conductive metal-oxide is demonstrated. As metal-oxide room-temperature-processed sol–gel SnO_x or Al:ZnO prepared by low-temperature (100 °C) atomic layer deposition is used, respectively. In this concept, the metal-oxide is intended to fuse the wires together and also to "glue" them to the substrate. As a result, a low sheet resistance down to 5.2 Ω sq^{-1} is achieved with a concomitant average transmission of 87%. The adhesion of the NWs to the substrate is significantly improved and the resulting composites withstand adhesion tests without loss in conductivity. Owing to the low processing temperatures, this concept allows highly robust, highly conductive, and transparent coatings even on top of temperature sensitive objects, for example, polymer foils, organic devices. These Indium- and PEDOT:PSS-free hybrid layers are successfully implemented as transparent top-electrodes in efficient all-solution-processed semitransparent organic solar cells. It is obvious that this approach is not limited to organic solar cells but will generally be applicable in devices which require transparent electrodes.

1. Introduction

Research towards transparent electronics has gained substantial momentum in recent years.[1] Transparent thin-film-transistors to drive transparent displays,[2] semitransparent organic light emitting diodes (OLEDs),[3] or see-through organic solar cells (OSCs)[4] that can even be integrated in windows open a wide spectrum of novel applications. Common key components of semitransparent devices are transparent electrodes. For this purpose, transparent conducting oxides (TCOs) have been widely explored.[5] Among them, indium tin oxide (ITO) has evolved as the most frequently used TCO. The limited abundance of Indium is expected to cause substantial issues in the not so far future. In a recent study, the ITO coated PET substrate was shown to account for a significant portion of the production costs and the energy consumption for production.[6] On temperature sensitive substrates, ITO suffers from a severely limited performance as ITO typically requires thermal treatment at $T > 300$ °C to achieve its optimum conductivity and transmittance at the same time.[7] Taken together, alternatives to ITO are desperately required.

A number of reports demonstrated an alternative concept based on oxide/metal/oxide transparent electrode structures, which can be prepared at room temperature (RT).[7,8] A drawback is the requirement for costly vacuum processing with potentially limited throughput. To increase throughput and to reduce manufacturing costs, solution based processing concepts for transparent conducting electrodes have become the subject of intense research. Carbon-based nanomaterials like graphene[9] and carbon nanotubes[10] have been considered and partially commercialized. In spite of a high average transmittance (T_{av}) in the visible spectral region of 80–90%, their moderate sheet resistivity (R_{sh}) on the order of 100–200 Ω sq^{-1} limits their applicability as a serious universal ITO-replacement.[11] Alternatively, transparent conducting layers based on metal nano-grids or random nanowire networks have been reported.[12] Among them, silver-nanowires (AgNWs) have attracted most of attention, for they are highly conductive, fairly stable and can be prepared with excellent control regarding wire geometry.[13] In their pioneering work, Lee et al. have used a simple drop casting technique to prepare AgNW meshes with T_{av} of 85% and a low R_{sh} of 10 Ω sq^{-1}.[14] To remove the dispersing agent (polyvinylpyrrolidone) used in their coating process and to improve the electrical connection between the wires, a heat treatment at 200 °C for several tens of minutes was required. A lowered resistance at the wire junctions was also achieved by electrochemical approaches.[15] A severe drawback of neat AgNW meshes is their limited adhesion to the substrate and their failure in conventional mechanical scotch-tape tests.[15] In addition, as the NWs typically cover less than 20% of the substrate, large open areas on the order of

K. Zilberberg, F. Gasse, R. Pagui, A. Polywka, A. Behrendt, S. Trost, Dr. R. Heiderhoff, Prof. P. Görrn, Prof. T. Riedl
Institute of Electronic Devices
University of Wuppertal
Rainer-Gruenter-Str. 21, 42119, Wuppertal, Germany
E-mail: t.riedl@uni-wuppertal.de

DOI: 10.1002/adfm.201303108

several μm^2 between the wires remain insulating. For a range of device applications the NW mesh electrode must be able to contact to the device all over the active area to allow for efficient charge extraction/injection. This is especially important for organic devices because of a typically small lateral conductivity in the organic semiconductor. To this end, the space between the AgNWs must be filled with a transparent and sufficiently conductive medium. Several attempts have been made by combining the AgNW-mesh with a conductive polymer, for example, PEDOT:PSS.[16] Unfortunately, PEDOT:PSS has been evidenced to initiate a number of degradation mechanisms in organic electronic devices like OLEDs or OSCs and to severely limit the device lifetime.[17] In an alternative approach, the AgNW mesh is coated with metal oxide nanoparticles (NPs), such as TiO_x,[16c] ZnO[18] or Al:ZnO (AZO).[19] As a substantial drawback, typically high annealing temperatures (140 °C to 250 °C) have been found to be necessary to sinter the NPs, to improve the adhesion to the substrate and to reduce the sheet resistance of the resulting layer. This impedes the application of these electrodes on top of temperature sensitive substrates or organic electronic devices. A low temperature approach based on a AgNW-TiO_2-PEDOT:PSS composite system has been reported.[20] However, issues introduced by PEDOT:PSS and its detrimental effects on device lifetime have been discussed above. Very recently, Yang's group has shown the use of ITO-NPs, deposited on top of the AgNW-mesh at RT without any post annealing.[21] Low-temperature processing of the transparent electrode allowed even the use as transparent top electrode of OSCs, and as a result highly efficient semitransparent OSCs have been demonstrated. Nevertheless, the applicability of this approach is somewhat voided by the use of ITO NPs and the issues related to Indium, as discussed above.

Therefore, in this work we present a PEDOT- and In-free hybrid approach for transparent, conductive and robust electrodes which can be prepared even at RT. To this end, we propose composite electrodes of AgNWs with either sol–gel processed tin-oxide ($sSnO_x$) or with Aluminum doped zinc oxide (AZO) prepared by atomic layer deposition (ALD). For the $sSnO_x$, we use a recently developed sol–gel process, that allowed us to prepare electron selective interlayers for inverted OSCs at temperatures as low as RT.[22] For the AgNW/AZO composite prepared by ALD, we want to note, that there is a strong current impetus to explore ALD for roll-to-roll (R2R), high-throughput production systems, even at atmospheric pressure.[23] Therefore, both presented approaches bear the potential for cost-effective manufacturing. We demonstrate for both cases, that the metal-oxide coating fuses the wires together which results in a significant reduction of R_{sh} from 90 Ω sq^{-1} for pristine AgNW meshes down to values as low as 5.2 Ω sq^{-1} at a concomitant average transmission (T_{av}) of 87% (referenced to glass). This is shown to be even superior to ITO electrodes. At the same time, the AgNW mesh is also conductively "glued" to the substrate which significantly improves the adhesion of the AgNW and guarantees an electrical contact to the entire area. The resulting composites withstand the mechanical adhesion tests without loss in conductivity. The application of the composite AgNW/$sSnO_x$ as transparent top electrode in efficient all-solution processed semitransparent OSCs is demonstrated.

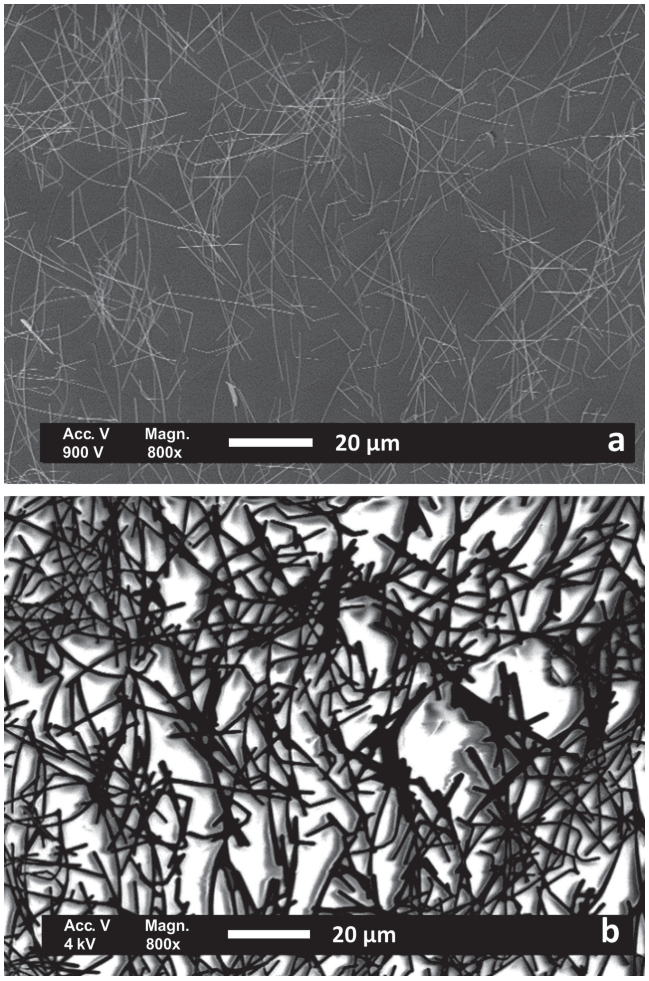

Figure 1. SEM-image of as-casted AgNW-mesh on glass taken at acceleration voltage of the primary electron beam of a) 900 V and b) 4 kV.

2. Results and Discussion

2.1. Ag-Nanowire/Metal-Oxide Composites

Figure 1a shows a SEM-image of the as-casted AgNW-mesh on a glass substrate taken at an acceleration voltage of 900 V. At this acceleration voltage the charging of the insulating glass substrate can be avoided, as the charge (introduced to the sample by the electron beam bombardment) is balanced by the charge that leaves the sample as secondary or backscattered electrons.[24] For higher acceleration energies (4 keV, Figure 1b), charging of the sample takes place in the open area of the AgNW mesh resulting in an electron beam induced potential contrast. The regions close to the conductive and grounded AgNW-mesh appear dark, as the excessive charge is transferred to the ground. In strong contrast, the regions in between the wires appear bright as lateral charge transport to the grounded NW mesh is impossible on the insulating glass, which leads to significant charging effects. This strikingly visualizes the inherent drawback of the neat AgNW mesh, which fails to

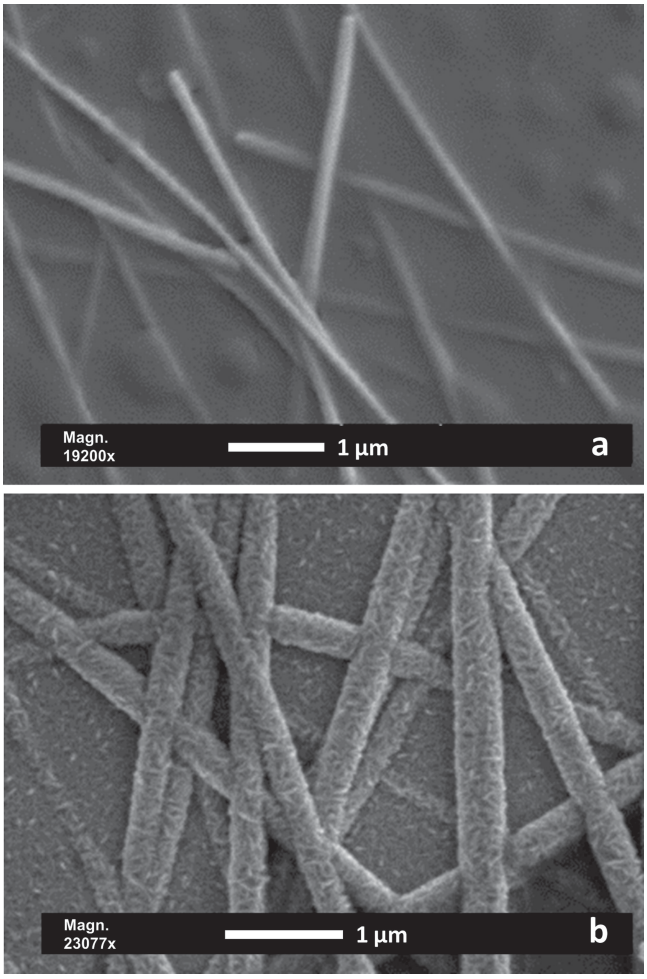

Figure 2. Magnified SEM-images of AgNWs coated with a) $sSnO_x$ and b) ALD-AZO.

electrically contact to the substrate all over and leaves non-contacted area, which would be detrimental for device applications.

To achieve an electronically functional contact to the entire substrate area, we fill the space between the wires with a moderately conductive metal-oxide using sol–gel processed $sSnO_x$ or Al:ZnO prepared by low-temperature (100 °C) atomic layer deposition (ALD). This is expected to allow for an effective charge extraction or injection over the active device area, which is required in an OLED or OSC. Details of the deposition process of the respective metal oxide can be found in the Experimental Section.

Coating the AgNW-mesh on glass with $sSnO_x$, a very effective fusion between AgNWs on their crossing points (see SEM image in **Figure 2**-a) and a dramatically reduced R_{sh} of 5.2 Ω sq^{-1} (from 90 Ω sq^{-1} for the neat AgNW-mesh) can be achieved. In a similar sense as for the AgNWs/$sSnO_x$ layers, the R_{sh} decreases to 31 Ω sq^{-1}, if the AgNW mesh is coated with AZO (**Table 1**). As one can see in the SEM image (Figure 2b), the AZO forms a nanocrystalline conformal coating on the pre-deposited AgNW mesh. The formation of nano-crystals is typical for ZnO layers, even if deposited at the low temperatures used in our ALD process.

Table 1. T_{av} (in range from 350 to 900 nm) and R_{sh} for composite layers of AgNWs and metal oxide. The data for specular and diffusive transmission at a wavelength of 632.8 nm is also given for the NW samples. The data for ITO prepared at room temperature (ITO_{RT})[7] is stated as a reference.

	AgNWs	AgNWs/SnO_x	AgNWs/AZO	ITO_{RT} (60 nm)
R_{sh} [Ω sq^{-1}]	90	5.2	31	83
T_{av} [%]	84	81	80	–
$T_{av\ (in\ ref.\ to\ glass)}$ [%]	90	87	86	85
$T_{specular\ at\ 632.8\ nm}$ [%]	79	72	72	–
$T_{specular}/T_{diffusive}$ [%]	82	81	77	–

It is important to note that AZO processed at 100 °C demonstrates an electrical conductivity of ≈10^{-1} S cm^{-1}, 3 orders of magnitude higher than that of $sSnO_x$ (≈10^{-4} S cm^{-1}). Nevertheless, the hybrid layers with $sSnO_x$ show even superior sheet conductivity. This clearly shows that the resulting R_{sh} of the composite layer is governed by the quality of the NW-to-NW junction, and the charge transport is dominated by the AgNW, whereas the metal-oxide only serves as a (moderately) conductive glue to join the wires with each other and to conductively fix the mesh to the entire substrate area.

The surface morphology of the AgNW/metal-oxide composite layers has been studied by atomic force microscopy (AFM) (see Figure S1, Supporting Information). The rms roughness of pristine AgNW layers is 65 nm (determined on a scan area of 50 µm × 50 µm). For the AgNW/$sSnO_x$ composite the roughness is reduced to 34 nm. In the case of the AgNW/AZO layer an increased roughness of 81 nm is found. This may be attributed to an added roughness due to the nano-crystalline ALD AZO and the fact that the conformal nature of the ALD coating process is not suitable to smoothen out a rough surface in a similar way as a solution based process. The conformal coating of the wires with AZO can be nicely seen in the AFM images (Supporting Information, Figure S1e,f) where an apparent increase of the wire thickness from the original value of 90 nm to roughly 90 nm plus twice the thickness of the AZO ALD layer (2 × 80 nm) is found. In the tapping phase image of Figure S1f (Supporting Information), the intrinsically rough morphology of the AZO layer due to the formation of crystallites can be seen in between the wires. We want to note, that we did not apply any deliberate planarization process, for instance, pressing, to reduce the surface-roughness of the NW layer and to avoid on even larger areas individual wires sticking out on the order of microns. Nevertheless, these well-established planarization concepts[15] could be combined with our approach previous to the deposition of the metal-oxide.

The optical properties of neat and hybrid structures are assessed by measuring their specular and scattered transmission. Details of the measurement are given in the supporting information. The mesh of stochastically distributed AgNWs causes a pronounced scattering of light incident under normal angle. Therefore, for a specific application, it is important to distinguish between the transmitted light that remains collimated (specular transmission) and the part of light that is transmitted

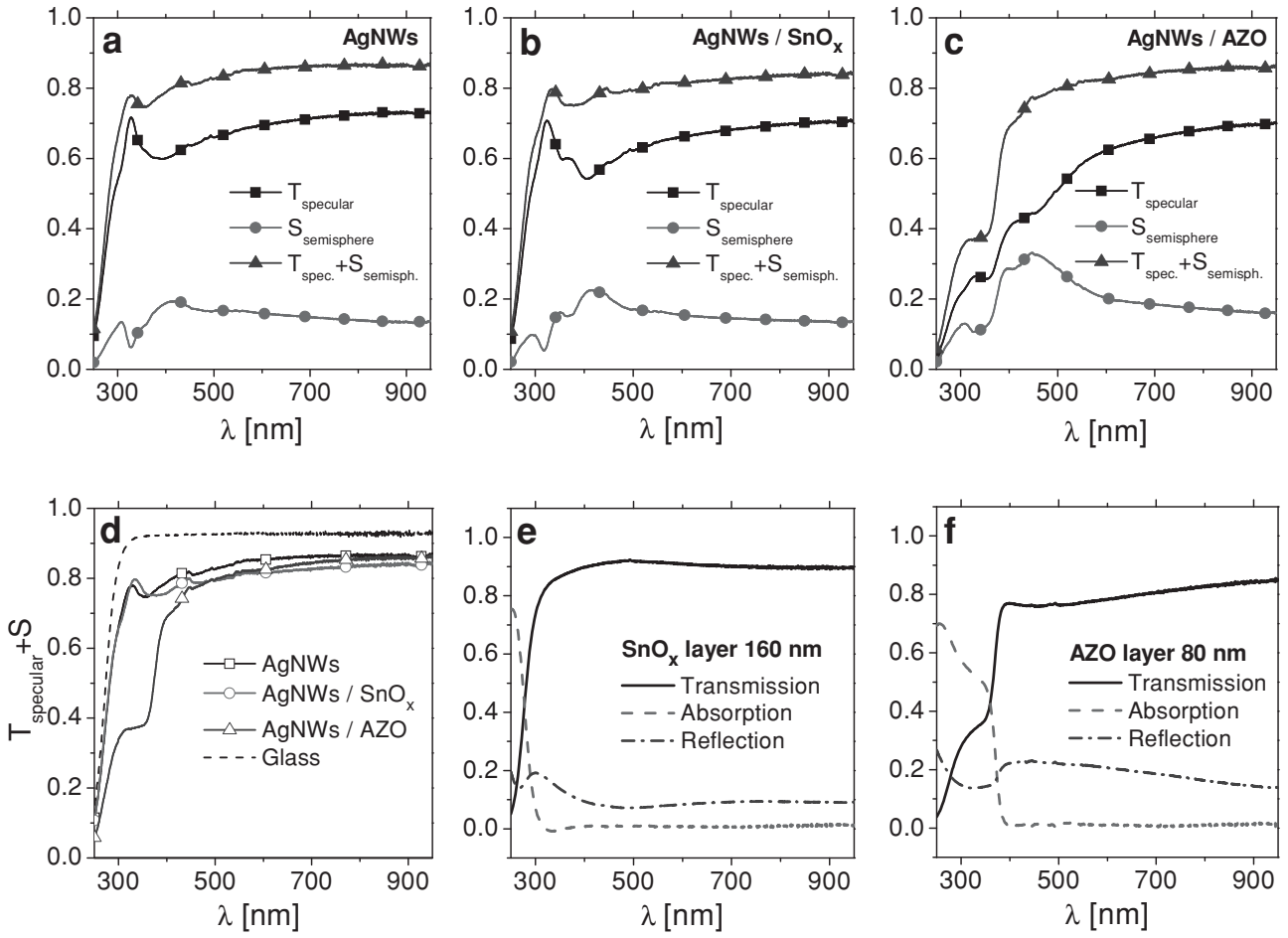

Figure 3. Plots of optical specular transmittance ($T_{specular}$), semisphere-scattered (detected in 45° angle, see Supporting Information) transmittance ($S_{semisphere}$), and the resulting total diffusive transmittance ($T_{specular}$ + $S_{semisphere}$) of a neat AgNW-mesh on a) glass, b) AgNWs/sSnO$_x$ hybrid layer, and c) AgNWs/ALD-AZO hybrid layer; d) comparison of the total diffusive transmittance of neat and metal-oxide coated AgNW-based electrodes on glass; e) transmission, absorption and reflection spectra of neat metal oxides sSnO$_x$ and f) ALD-AZO on glass substrate.

but scattered to other angles. To specifically evaluate this, the optical transmission of hybrid layers was measured at different distances and angles (see Supporting Information) using a HeNe-laser as a source of collimated light (4 mW, 632.8 nm). The corresponding specular transmittance and its ratio to the diffusive (total) transmittance into the half sphere behind the substrate are listed in the Table 1. At 632 nm, 72% of incident light is transmitted through both hybrid layers (AgNW/sSnO$_x$ and AgNW/AZO) without scattering.

For the non-coated AgNWs layers, a characteristic maximum of the specular transmission (**Figure 3**a) is found at 325 nm (characteristic plasma frequency of silver). At larger wavelengths the transmission shows a slight decrease which correlates with the scattering spectra. As discussed in the supporting information this is due to the well-known effect of surface plasmon polariton scattering.[25] Note, T_{av} is defined as the sum of specular and scattered transmittance (Figure 3a). It is 84% (or 90% when the glass substrate is used as reference) in the case of the neat AgNW layer.

For the AgNWs/sSnO$_x$ composite, it is important to note that sSnO$_x$ has an absorption edge at 300 nm (Figure 3e), and therefore is highly transparent in visible region. Thus, the composite AgNW/sSnO$_x$ is expected to remain unaffected by any intrinsic absorption of the sSnO$_x$. A spectral minimum in the specular transmission spectrum appears at 420 nm for AgNWs/sSnO$_x$ layers (Figure 3b). This is due to light scattering in the hybrid system (see Supporting Information for more details). T_{av} remains largely unaffected high (Table 1) at 81% (or when a glass substrate is used as reference: 87%) in the AgNWs/sSnO$_x$ composite. Note, the high transmittance together with a low R_{sh} of 5.2 Ω sq^{-1} positions AgNW/sSnO$_x$ composites among the best metal-nanowire based transparent electrodes, reported to date (see Figure S4, Supporting Information). In contrast to these previous results, which have typically been obtained by thermal post processing of the Ag NW at temperatures of 140 °C and above, the highest temperature in the preparation of our AgNW/sSnO$_x$ composites has been as low as 50 °C.

A substantially enhanced scattering of light is found for the AgNWs/AZO hybrid layer (Figure 3c) compared to AgNWs/sSnO$_x$ (Figure 3b). It is known that the particle plasmon resonance wavelength and thereby also the average extinction are increased with increasing refractive index of the particle

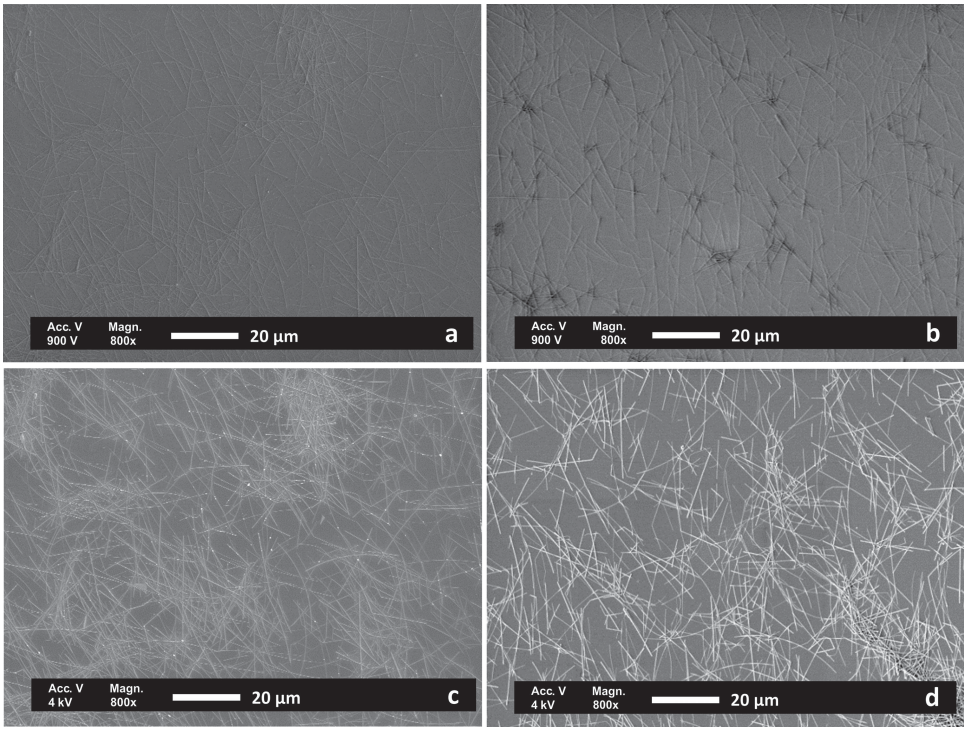

Figure 4. SEM-images of composite layers of a,c) AgNWs and $sSnO_x$ or b,d) ALD-AZO at 900 V and 4 kV, respectively.

environment.[27] We therefore assume that a similar effect applies for AgNW. Thus, when pure AgNW films are coated with tin oxide the environment is changing from air/glass to SnO_x/glass. Due to the increase of the refractive index of the environment (for SnO_x, n = 1.62 @ 500 nm), the AgNW plasmon resonance wavelength is increased from 390 nm to 407 nm. Both, extinction and scattering are increased. When coated with AZO (n = 2.04 @ 500 nm) the refractive index is further increased and so are extinction and scattering. Comparing these spectra one has to keep in mind that AZO shows a fundamental absorption below 388 nm (Figure 3f). At smaller wavelengths, the extinction of light is dominated by the fundamental absorption in AZO. At larger wavelengths, the excitation of SPPs is responsible for light extinction. With this in mind it becomes clear that again scattering and extinction show a very similar spectrum. For an organic solar cell, elastic hemisphere scattering could be utilized to optimize light in-coupling dramatically (especially at low light intensities).

Owing to the intrinsic absorption of the AZO layers (Figure 3f), the overall transmittance of the AZO-coated mesh electrode in the spectral region below 388 nm is dominated by the absorption due to AZO. Therefore, a somewhat lower total optical transmittance T_{av} of 80% (or 86%, if in ref. to a glass substrate) was determined for AgNWs/AZO layers. Note, 60 nm of ITO sputtered at RT[7] only exhibits $T_{av\ (ref.\ to\ glass)}$ of 85% and a concomitantly high R_{sh} of 83 Ω sq^{-1} (Table 1). Figure 3d summarizes and compares the total optical transmittances for AgNWs-meshes, hybrid layers, and a glass substrate.

Figure 4a,b shows the SEM-images of composite AgNWs/sSnO*x* and AgNWs/AZO layers respectively at a primary electron beam acceleration voltage of 900 V. The corresponding SEM images of composite layers taken at higher acceleration voltages of 4 kV (Figure 4c,d) do not show the electron beam induced potential contrast (they show material contrast only), as the charge introduced between the AgNWs can now be transported to the highly conductive grounded AgNW-mesh. This is in stark contrast to the results for uncoated AgNW meshes (see Figure 1).

In addition to a conductive connection to the substrate, the mechanical adhesion of the composite is dramatically superior to that of the uncoated mesh. This is favorably verified by a scotch-tape peeling test, with the corresponding results shown in the photographs of **Figure 5**. Whereas the pristine AgNW mesh is easily peeled off (Figure 5a,c) by the scotch tape, the AgNW/$sSnO_x$ composite is outstandingly stable (Figure 5b,d). A similar mechanical stabilization is achieved for the AgNW/AZO composite system (not shown here). While the pristine sample no longer shows any conductivity after peeling, the composite electrodes remain unaffected by the peeling test. It must furthermore be noted that aging tests of the composite electrodes in a climate cabinet (80 °C/80% rH) for a week left their R_{sh} unchanged (Supporting Information, Table S1). This is a very encouraging result when the application of these electrodes in a more demanding environment is considered.

2.2. Semi-Transparent Organic Solar Cell with Hybrid Top-Electrode

The favorable properties of our hybrid layers are exemplary demonstrated for the AgNW/$sSnO_x$ composite used

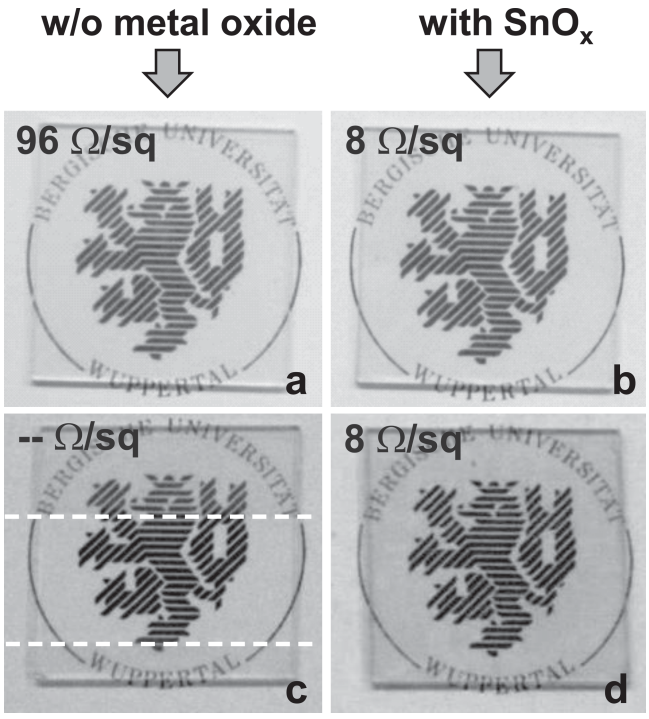

Figure 5. AgNWs w/o metal oxide a) before and c) after scotch-tape peeling test. The peeled-off region is between the two dashed lines; AgNWs with $sSnO_x$ b) before and d) after the scotch-tape peeling test.

as a top electrode in efficient semitransparent inverted polymer:fullerene OSCs (**Figure 6**a,d,e, **Table 2**). As detailed above, we did not apply any deliberate planarization process, such as pressing, to reduce the surface-roughness of the NW layer and to avoid individual wires sticking out. Thus, to avoid short circuits our AgNW/metal-oxide composites have been used as top-electrodes in the semi-transparent organic solar cells. The inverted cell set-up with anode side on top has been chosen, as this architecture has previously been shown to be attractive for manufacturing and for better device lifetime.[28]

The work-function of SnO_x and AZO used in the composite electrodes is 4.1 eV and 4.0 eV, respectively.[22,29] Thus, a-priori, this rather low WF would render our electrodes more favorable to extract electrons rather than holes from typical organic solar cell active materials. However, to facilitate hole extraction via these composites in our devices, we used high-WF metal oxide interlayers (vanadium oxide or molybdenum oxide), which have previously been evidenced to favorably interface to the HOMO level of many organic semiconductors used in OLEDs and OSCs. When inserted between the organic active layer and the actual anode, they alleviate the need to select an anode material with an appropriate WF.[30]

The inverted OSCs studied in this work have the following layer sequence: glass/TCO/sol–gel-TiO_x/P3HT:$PC_{60}BM$ (200 nm)/sol–gel-VO_x or evaporated-MoO_3/(AgNW/$sSnO_x$) for the semi-transparent device or Al/Ag for the opaque reference device. For VO_x (50 nm) we used a sol–gel process, as we have recently reported.[26a] Aside from the transparent AgNW/$sSnO_x$ top electrode, the inverted cells with an active area of 3 mm^2 are identical to previous reports.[26b] As an alternative to the sol–gel VO_x, a thermally evaporated MoO_3 layer (80 nm) was deposited on top of BHJ. The AgNWs dispersion (5 mg mL^{-1}) and the sol–gel solution for $sSnO_x$ were deposited sequentially under N_2-atmosphere by spin-coating. Note, as bottom electrode TCO we either used ITO or F:SnO_2.

A high transmittance of >75% for the entire semitransparent cell is found in the red spectral region ($\lambda > 650$ nm) (Figure 6c), independent of the illumination side. The corresponding OSC performance characteristics are summarized in Table 2. While a typical efficiency of 3% is found for the opaque reference devices, the semitransparent cells show efficiencies up to 2.5%. A higher J_{sc} is measured for illumination from the glass side compared to top illumination through the AgNW/$sSnO_x$ electrode. We attribute the lower J_{sc} in the latter case to scattering effects that take place in the AgNW/$sSnO_x$. We have to stress, that the cells have not been optimized to harvest the above discussed light scattering effects of the AgNW/$sSnO_x$ mesh for improved light trapping. Somewhat lower J_{sc} is encountered for all-solution processed devices with sVO_x/AgNWs/$sSnO_x$ anode due to the parasitic absorption in 50 nm thick bulk of VO_x. Note, VO_x exhibits an absorption edge already at 540 nm.[26] In any case, the fill factors of our AgNW-based semitransparent devices with both hole-extraction interlayers of $eMoO_3$ and sVO_x are similar. Note, the series resistance R_s of the OSCs increases from about 2 Ω cm^2 for the opaque reference devices with an evaporated metal top electrode to about 4 Ω cm^2 for the semitransparent devices based on AgNW/metal-oxide composite electrodes. In spite of the low sheet resistance of the AgNW/SnO_x electrodes, this factor of two increased series resistance may be explained by a non-optimized interface between SnO_x and the high-WF hole extraction interlayers VO_x or MoO_x. Note, in previous reports on using PEDOT:PSS/AgNW top electrodes, a factor of 5 increase of R_s compared to that of the opaque reference was evidenced and explained in part by a limited contact of the mesh electrode to the active device area.[16d] In this respect, even in non-optimized devices our composite electrodes already outperform this previous work. To demonstrate the viability of entirely In-free semi-transparent OSCs, we have also prepared devices with F:SnO_2 as bottom electrode. Their device characteristics are essentially similar to that of the ITO based cells (Table 2).

3. Conslusions

We demonstrated transparent electrodes based on composites of silver nanowires and conductive metal-oxides (sol–gel SnO_x processed at room temperature or moderate temperature ALD-processed AZO). The coating with these thin conductive metal-oxides results in a sheet resistance of the composite as low as 5.2 Ω sq^{-1} with a concomitant high average optical transmission of 87%. At the same time, the adhesion of AgNWs on the substrate is significantly improved. Importantly, the NW/metal-oxide composites allow for electrical contacting devices all over the active area. Their low processing temperature enables the application of these transparent conductive composites as top-electrodes of organic devices. This is exemplified in efficient, In- and PEDOT:PSS-free, all-solution processed semitransparent organic solar cells.

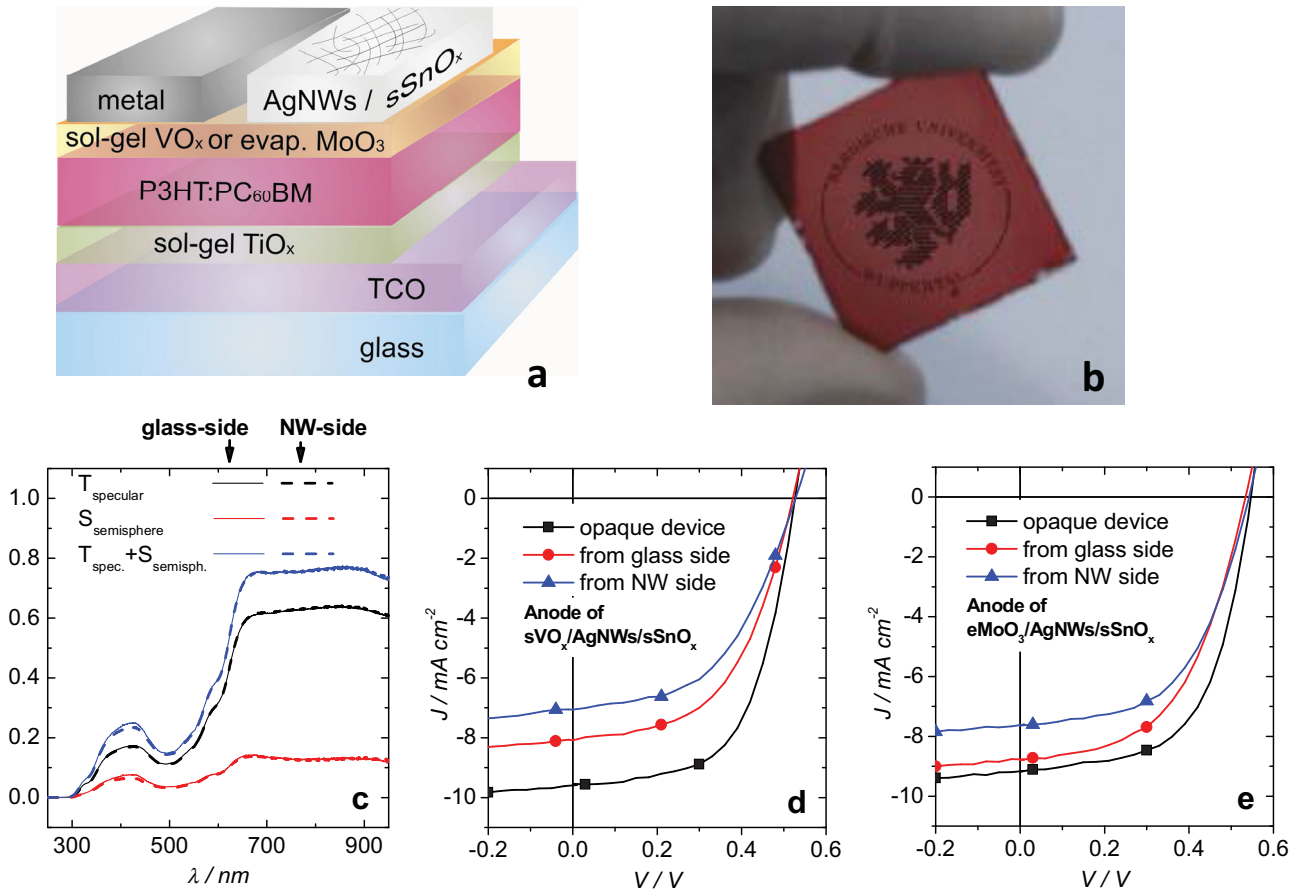

Figure 6. a) Layer sequence of the inverted OSCs. b) Photo of a large-area device stack with an anode of sVO_x/AgNWs/$sSnO_x$. c) Optical transmission spectrum ($T_{specular}$, scattered transmission $S_{semisphere}$, and their superposition $T_{spec.}$+ $S_{semisph.}$) of the OSC-stack illuminated from glass side and from the AgNW/$sSnO_x$ top contact side. d) *J–V* characteristics of all-solution processed semitransparent inverted polymer:fullerene OSC with sVO_x/AgNWs/$sSnO_x$ anode and opaque reference device with sVO_x/Al/Ag anode. e) *J–V* characteristics of semitransparent inverted polymer:fullerene OSC with $eMoO_3$/AgNWs/$sSnO_x$ anode and opaque reference device with $eMoO_3$/Al/Ag anode. Note, the bottom TCO electrode was ITO in this set of samples.

4. Experimental Section

It is known that T_{av} and R_{sh} of AgNW-meshes can be tuned over a certain range by simply varying the concentration of NWs in the dispersion. In this work, the initial AgNW dispersion (Blue Nano, conc. 10 mg mL^{-1}, diameter 90 nm, length > 20 µm) without any polymeric stabilizer was further diluted with a dry IPA to a final concentration of 5 mg mL^{-1}. The AgNW-mesh was spin coated from a well-shaked and ultra-sonicated (30 s) AgNW-dispersion in air and dried at 50 °C for 1 min to remove the solvent. For the sol–gel deposition of $sSnO_x$, Tetrakis-(dimethylamino)tin (TDMASn) has been used as precursor in isopropanol. Acetylacetone was used as stabilizing additive. Previous to spincoating, the solution was stirred at RT and 60% rH for 30 min. Condensation (film formation) took place at RT at 60% rH. More details can be found elsewhere.[22] AZO layers were prepared as ALD nano-laminates of a repeated deposition of 50 cycles ZnO and 2 cycles Al_2O_3 at 100 °C using a BENEQ TFS 200 system. Details of the AZO preparation and characterization can be found in our previous report.[3a] If not otherwise stated in the manuscript, we chose deposition parameters for the coating of the metal oxides on top of the cast AgNW-mesh, that on planar glass substrates (without the NW mesh) would yield a metal-oxide layer thickness of 80 nm.

Table 2. Characteristics of semitransparent inverted polymer:fullerene OSC with liquid-processed AgNW/$sSnO_x$ top contact and opaque reference device with thermally evaporated metallic top contact.

Inverted P3HT:$PC_{60}BM$ OSCs		PCE [%]	V_{oc} [V]	J_{sc} [mA cm^{-2}]	FF [%]
ITO/$sTiO_x$/BHJ/sVO_x/Al/Ag (opaque reference)		3.0	0.53	9.6	59
ITO/$sTiO_x$/BHJ/sVO_x/AgNWs/$sSnO_x$	glass side	2.2	0.52	8.1	53
	NW side	1.9	0.53	7.1	50
ITO/$sTiO_x$/BHJ/$eMoO_3$/Al/Ag (opaque reference)		3.0	0.55	9.2	59
ITO/$sTiO_x$/BHJ/$eMoO_3$/AgNWs/$sSnO_x$	glass side	2.5	0.53	8.8	52
	NW side	2.2	0.54	7.6	54
F:SnO_2/$sTiO_x$/BHJ/$eMoO_3$/AgNWs/$sSnO_x$	glass-side	2.4	0.53	8.8	51
	NW side	2.0	0.52	7.7	50

MoO_3 was thermally evaporated from the effusion cell at the temperature 615 °C and corresponding deposition rate of 0.04 nm s^{-1}. For entirely In-free, semi-transparent OSCs we have used F:SnO_2 substrates with a sheet resistance of 13 Ω sq^{-1}. (Sigma Aldrich). The *J–V* characteristics of OSCs were measured under 100 mW cm^{-2} AM1.5G spectrum of solar simulator (Newport, 300 W) using Keithley 2400-C SMU. The SEM study was done using a Philips XL30S FEG microscope with a field emission cathode. The electrical conductivity

of AZO was determined via 4-probe-methode. The conductivity of less conductive SnO_x was determined from *I–V* curves measured on pre-patterned ITO/Au inter-digitated µm-structures with defined geometry covered with sol–gel SnO_x.

Supporting Information

Supporting Information is available from the Wiley Online Library or from the author.

Acknowledgements

The authors are grateful to S. Adamczyk from the Department of Macromolecular Chemistry (University of Wuppertal, Germany) for carrying out the AFM measurements. The authors thank the German Federal Ministry for Education and Research (Grant No. 13N11777) and the Deutsche Forschungsgemeinschaft (DFG) (Grant: RI1551/4–1) for financial support. Honeywell Specialty Chemicals Seelze GmbH is acknowledged for the generous supply with P3HT. P.G. acknowledges funding by the Emmy-Noether-Programm of the DFG (Deutsche Forschungsgemeinschaft).

Received: September 6, 2013
Published online: November 20, 2013

[1] a) J. F. Wager, *Science* **2003**, *300*, 1245–1246; b) T. Marks, A. Facchetti, *Transparent Electronics: From Synthesis to Applications*, John Wiley & Sons, West Sussex **2010**; c) R. Martins, E. Fortunato, P. Barquinha, L. Pereira, *Transparent Electronics: From Materials to Devices.*, John Wiley & Sons, West Sussex **2012**.
[2] P. Görrn, M. Sander, J. Meyer, M. Kroger, E. Becker, H. H. Johannes, W. Kowalsky, T. Riedl, *Adv. Mater.* **2006**, *18*, 738.
[3] a) J. Meyer, P. Görrn, S. Hamwi, H. H. Johannes, T. Riedl, W. Kowalsky, *Appl. Phys. Lett.* **2008**, *93*, 073308; b) J. Meyer, T. Winkler, S. Hamwi, S. Schmale, H. H. Johannes, T. Weimann, P. Hinze, W. Kowlasky, T. Riedl, *Adv. Mater.* **2008**, *20*, 3839.
[4] H. Schmidt, H. Flügge, T. Winkler, T. Bulow, T. Riedl, W. Kowalsky, *Appl. Phys. Lett.* **2009**, *94*, 243302.
[5] a) J. R. Bellingham, W. A. Phillips, C. J. Adkins, *J. Mater. Sci. Lett.* **1992**, *11*, 263–265; b) E. Fortunato, D. Ginley, H. Hosono, D. C. Paine, *MRS Bull.* **2007**, *32*, 242–247; c) D. S Ginley, C. Bright, *MRS Bull.* **2000**, *25*, 15–18; d) T. Minami, *MRS Bull.* **2000**, *25*, 38–44.
[6] a) A. J. Medford, M. R. Lilliedal, M. Jorgensen, D. Aaro, H. Pakalski, J. Fyenbo, F. C. Krebs, *Opt. Express* **2010**, *18*, A272–A285; b) N. Espinosa, R. García-Valverde, A. Urbina, F. Lenzmann, M. Manceau, D. Angmo, F. C. Krebs, *Sol. Energy Mater. Sol. Cells* **2012**, *97*, 3–13.
[7] T. Winkler, H. Schmidt, H. Flügge, F. Nikolayzik, I. Baumann, S. Schmale, T. Weimann, P. Hinze, H. H. Johannes, T. Rabe, S. Hamwi, T. Riedl, W. Kowalsky, *Org. Electron.* **2011**, *12*, 1612–1618.
[8] H. Jin, C. Tao, M. Velusamy, M. Aljada, Y. Zhang, M. Hambsch, P. L. Burn, P. Meredith, *Adv. Mater.* **2012**, *24*, 2572–2577.
[9] J. Wu, M. Agrawal, H. A. Becerril, Z. Bao, Z. Liu, Y. Chen, P. Peumans, *ACS Nano* **2009**, *4*, 43–48.
[10] a) D. Zhang, K. Ryu, X. Liu, E. Polikarpov, J. Ly, M. E. Tompson, C. Zhou, *Nano Lett.* **2006**, *6*, 1880–1886; b) Z. Wu, Z. Chen, X. Du, J. M. Logan, J. Sippel, M. Nikolou, K. Kamaras, J. R. Reynolds, D. B. Tanner, A. F. Hebard, A. G. Rinzler, *Science* **2004**, *305*, 1273–1276.
[11] a) J. K. Wassei, R. B. Kaner, *Mater. Today* **2010**, *13*, 52–59; b) L. Hu, D. S. Hecht, G. Grüner, *Chem. Rev.* **2010**, *110*, 5790–5844; c) F. Mirri, A. W. K. Ma, T. T. Hsu, N. Behabtu, S. L. Eichmann, C. C. Young, D. E. Tsentalovich, M. Pasquali, *ACS Nano* **2012**, *6*, 9737–9744.
[12] L. Hu, H. Wu, Y. Cui, *MRS Bull.* **2011**, *36*, 760–765.
[13] S. M. Bergin, Y.-H. Chen, A. R. Rathmell, P. Charbonneau, Z.-Y. Li, B. J. Wiley, *Nanoscale* **2012**, *4*, 1996–2004.
[14] J.-Y. Lee, S. T. Connor, Y. Cui, P. Peumans, *Nano Lett.* **2008**, *8*, 689–692.
[15] L. Hu, H. S. Kim, J.-Y. Lee, P. Peumans, Y. Cui, *ACS Nano* **2010**, *4*, 2955–2963.
[16] a) L. Yang, T. Zhang, H. Zhou, S. C. Price, B. J. Wiley, W. You, *ACS Appl. Mater. Inter.* **2011**, *3*, 4075–4084; b) J. Krantz, M. Richter, S. Spallek, E. Spiecker, C. J. Brabec, *Adv. Funct. Mater.* **2011**, *21*, 4784–4787; c) D.-S. Leem, A. Edwards, M. Faist, J. Nelson, D. D. C. Bradley, J. C. de Mello, *Adv. Mater.* **2011**, *23*, 4371–4375; d) J. Krantz, T. Stubhan, M. Richter, S. Spallek, I. Litzov, G. J. Matt, E. Spiecker, C. J. Brabec, *Adv. Funct. Mater.* **2013**, *23*, 1711.
[17] a) E. Voroshazi, B. Verreet, T. Aernouts, P. Heremans, *Sol. Energy Mater. Sol. Cells* **2011**, *95*, 1303–1307; b) M. Jorgensen, K. Norrman, S. A. Gevorgyan, T. Tromholt, B. Andreasen, F. C. Krebs, *Adv. Mater.* **2012**, *24*, 580–612.
[18] a) F. S. F. Morgenstern, D. Kabra, S. Massip, T. J. K. Brenner, P. E. Lyons, J. N. Coleman, R. H. Friend, *Appl. Phys. Lett.* **2011**, *99*, 183307; b) J. Ajuria, I. Ugarte, W. Cambarau, I. Etxebarria, R. Tena-Zaera, R. Pacios, *Sol. Energy Mater. Sol. Cells* **2012**, *102*, 148–152.
[19] T. Stubhan, J. Krantz, N. Li, F. Guo, I. Litzov, M. Steidl, M. Richter, G. J. Matt, C. J. Brabec, *Sol. Energy Mater. Sol. Cells* **2012**, *107*, 248–251.
[20] R. Zhu, C.-H. Chung, K. C. Cha, W. Yang, Y. B. Zheng, H. Zhou, T.-B. Song, C.-C. Chen, P. S. Weiss, G. Li, Y. Yang, *ACS Nano* **2011**, *5*, 9877–9882.
[21] a) C.-H. Chung, T.-B. Song, B. Bob, R. Zhu, H.-S. Duan, Y. Yang, *Adv. Mater.* **2012**, *24*, 5499–5504; b) L. Dou, W.-H. Chang, J. Gao, C.-C. Chen, J. You, Y. Yang, *Adv. Mater.* **2012**, *25*, 825–831; c) C.-C. Chen, L. Dou, R. Zhu, C.-H. Chung, T.-B. Song, Y. B. Zheng, S. Hawks, G. Li, P. S. Weiss, Y. Yang, *ACS Nano* **2012**, *6*, 7185–7190.
[22] S. Trost, K. Zilberberg, A. Behrendt, T. Riedl, *J. Mater. Chem.* **2012**, *22* (32), 16224–16229.
[23] a) E. Dickey, W. A. Barrow, *J. Vac. Sci. Technol. A* **2012**, *30* (2); b) S. F. Nelson, D. H. Levy, L. W. Tutt, M. Burberry, *J. Vac. Sci. Technol. A* **2012**, *30*, 01A154.
[24] a) L. Reimer, Scanning microscopy, *Physics of Image Formation and Microanalysis*, Springer Series in Optical Sciences, *45*, Springer Berlin **1985**; b) C. Thomas, I. Joachimsthaler, R. Heiderhoff, L. J. Balk, *J. Phys. D: Appl. Phys.* **2004**, *37*, 2785–2794.
[25] K. Aslan, Z. Leonenko, J. R. Lakowicz, C. D. Geddes, *J. Fluoresc.* **2005**, *15*, 643–654.
[26] a) K. Zilberberg, S. Trost, H. Schmidt, T. Riedl, *Adv. Energy Mater.* **2011**, *1*, 377–381; b) K. Zilberberg, S. Trost, J. Meyer, A. Kahn, A. Behrendt, D. Lützenkirchen-Hecht, R. Frahm, T. Riedl, *Adv. Funct. Mater.* **2011**, *21*, 4776–4783.
[27] a) K. L. Kelly, E. Coronado, L. L. Zhao, G. C. Schatz, *J. Phys. Chem. B* **2003**, *107*, 668–677; b) M. K. Kinnan, S. Kachan, C. K. Simmons, G. Chumanov, *J. Phys. Chem. C* **2009**, *113*, 7079–7084.
[28] F. C. Krebs, *Sol. Energ. Mat. Sol. C* **2009**, *93*, 465.
[29] S. Trost, K. Zilberberg, A. Behrendt, A. Polywka, P. Görrn, P. Reckers, J. Maibach, T. Mayer, T. Riedl, *Adv. Energy Mater.* **2013**, DOI: 10.1002/aenm.201300402.
[30] a) J. Meyer, S. Hamwi, M. Kröger, W. Kowalsky, T. Riedl, A. Kahn, *Adv. Mater.* **2012**, *24*, 5408; b) M. Kröger, S. Hamwi, J. Meyer, T. Riedl, W. Kowalsky, A. Kahn, *Appl. Phys. Lett.* **2009**, *95*, 123301.